Catalysis Communications 26 (2012) 103–111

Contents lists available at SciVerse ScienceDirect

Catalysis Communications

journal homepage: www.elsevier.com/locate/catcom

Short Communication

The effect of precipitants on Ni-Al_2O_3 catalysts prepared by a co-precipitation method for internal reforming in molten carbonate fuel cells

You-Shick Jung [a,b], Wang-Lai Yoon [a], Yong-Seog Seo [a,*], Young-Woo Rhee [b,**]

[a] Korea Institute of Energy Research, 71-2 Jang-dong, Yusung-gu, Daejeon 305-343, South Korea
[b] Department of Chemical Engineering, Chungnam National University, 220 Gung-dong, Yusung-gu, Daejeon 305-764, South Korea

ARTICLE INFO

Article history:
Received 2 March 2012
Received in revised form 24 April 2012
Accepted 27 April 2012
Available online 3 May 2012

Keywords:
Molten carbonate fuel cell (MCFC)
Ni-Al_2O_3 catalyst
Precipitant
Co-precipitation
Homogeneous precipitation

ABSTRACT

Ni-Al_2O_3 catalysts are prepared via the co-precipitation method using various precipitants: urea, Na_2CO_3, NaOH, K_2CO_3, KOH and NH_4OH. The effects of the precipitants on the physicochemical properties and catalytic activities of the Ni-Al_2O_3 catalysts are investigated. The Ni50-urea catalyst displays the largest specific surface area and the highest pore volume. This catalyst also exhibits the highest Ni dispersion and the largest Ni surface area. Ni50-urea catalyst prepared with urea as precipitant and Ni50-K_2CO_3 catalyst prepared with K_2CO_3 as precipitant exhibit high pore volumes and good catalytic activities for methane steam reforming. The Ni50-urea catalyst exhibits the best physicochemical properties and shows good catalytic activity and a strong resistance to electrolyte contamination.

1. Introduction

Fuel cells have attracted significant attention as new electric power systems in recent years [1]. The hydrogen required for fuel cells is primarily supplied from the steam reforming of hydrocarbons (i.e., methane, liquefied natural gas (LNG), ethanol) [2–4]. Ni or noble-metal (Pt, Ru) catalysts have traditionally been used for the steam reforming process [3–5]. However, Ni catalysts have been most widely used because of their outstanding merits with respect to cost and catalytic activity. Molten carbonate fuel cells (MCFCs) classified according to how the hydrogen is supplied to the stack system: external reforming (ER-MCFC), direct internal reforming (DIR-MCFC), and indirect internal reforming (IIR-MCFC) [7,10,11].

The DIR-MCFC has a strong advantage over the other two systems because of effective thermal management of the stack cell. In DIR-MCFCs, the steam reforming of methane and the electrochemical reaction occur simultaneously in the anode of the stack cell. The reforming reaction is endothermic; thus, the steam reforming within the stack cell is sustained by the heat released from the electrochemical reaction [9–11]. Methane steam-reforming systems are typically operated at 700 to 800 °C; however, the internal reforming reaction in molten carbonate fuel cells occurs at the relatively low temperature between 580 and 650 °C at which the stack cell is operated. Therefore, the catalyst for internal reforming requires a very high catalytic activity.

Despite their previously discussed advantages, DIR-MCFCs face several obstacles. The internal reforming catalysts placed in the anode channel are deactivated by the molten carbonate electrolyte (Li_2CO_3/K_2CO_3) [6–8,10–16]. Many researchers have studied the deactivation of internal reforming catalysts by molten carbonate electrolyte. Sugiura et al. [14] reported that the deactivation of internal reforming catalysts was mainly attributed to the pollution of the alkali electrolyte through the vapor phase, especially by t the catalyst of Ni particles under an atmosphere contaminated with alkali metals. Ito et al. [15] also suggested that internal reforming catalysts were heavily deactivated by K ions in the electrolyte.

Many studies have been conducted to develop internal reforming catalysts with a strong resistance to K- or/and Li-containing species in the electrolyte vapor. These catalysts have been prepared by various methods, including sol–gel [17,18], impregnation [19,20], co-precipitation [21–23] and sequential precipitation [24]. Among these preparation methods, the co-precipitation method is considered to be one of the most effective preparation methods for catalysts with highly dispersed and active particles that are suitable for internal reforming catalysts in DIR-MCFCs [10,25].

The catalysts prepared by the co-precipitation method exhibit good activity for the reforming reaction in DIR-MCFC tests. However, these catalysts exhibit different characteristics according to the precipitants. Thus, the selection of a precipitant is very important. In general, precipitants used in the co-precipitation method are sodium

* Corresponding author. Tel.: +82 42 860 3612.
** Corresponding author.
E-mail addresses: ysseo@kier.re.kr (Y-S. Seo), ywrhee@cnu.ac.kr (Y-W. Rhee).

1566-7367 Published by Elsevier B.V. Open access under CC BY-NC-ND license.
doi:10.1016/j.catcom.2012.04.029

carbonate, sodium hydroxide, ammonia solution, urea, and others. However, the literature contains few studies on Ni-Al_2O_3 catalysts prepared by co-precipitation with various types of precipitants for the purpose of being used in a DIR-MCFC; thus, it is necessary to investigate the characteristics of the Ni-Al_2O_3 catalysts with various precipitants under atmospheres poisoned with the electrolytes used in DIR-MCFCs. In this study, we have examined the effects of various precipitants on the physicochemical properties and catalytic performance of Ni-Al_2O_3 catalysts prepared by co-precipitation.

2. Experimental

2.1. Preparation of catalysts

The Ni-Al_2O_3 catalysts were prepared via the co-precipitation method using various precipitants. The precipitants were urea ($(NH_2)_2CO$), sodium carbonate (Na_2CO_3), sodium hydroxide (NaOH), potassium carbonate (K_2CO_3), potassium hydroxide (KOH) and ammonia solution (NH_4OH). These precipitants can be classified according to their functional groups into the carbonate-ion group and the hydroxide-ion group. The carbonate-ion group includes sodium carbonate, potassium carbonate and urea. In cases where the urea solution was decomposed into ammonium (NH_4^+) and carbonate (CO_3^{2-}) ions at 80–100 °C, which corresponds to the synthesis temperature, the urea can then be classified as a member of the carbonate-ion group. The hydroxide-ion group includes sodium hydroxide, potassium hydroxide and ammonia solution.

Solutions of nickel and aluminum nitrate were prepared via the dissolution of $Ni(NO_3)_2 \cdot 6H_2O$ and $Al(NO_3)_3 \cdot 9H_2O$ in distilled water. The nickel nitrate concentration and aluminum nitrate concentration were fixed at 0.085 mol L^{-1} and 0.098 mol L^{-1}, respectively. The precipitants were also prepared by dissolution in distilled water. The concentration of the urea solution was fixed at 6 mol L^{-1}. The concentrations of the sodium carbonate and potassium carbonate solutions were both fixed at 0.3 mol L^{-1}. The concentrations of the precipitants that contained hydroxide ions were fixed at 0.6 mol L^{-1}. Each precipitant exhibited differences in concentration according to the functional group of the precipitant, with the exception of urea, because the members of the hydroxide-ion group contain 1 equivalent of alkali ions, whereas the members of the carbonate-ion group contain 2 equivalents of ions.

In the case of urea, solutions of the metal nitrates and urea were mixed in a 2 L reactor equipped with a thermocouple, and the resulting solution was maintained at 85 °C for 10 h under vigorous stirring; the pH of this solution was maintained at 7 [9,26]. For other catalysts, solutions of the metal nitrates were placed in a 2 L reactor equipped with a thermocouple, and the solution was maintained at 85 °C for 10 h with vigorous stirring. The solutions of precipitants were then placed in a 2 L reactor, and their pH values were adjusted to 10 except for the catalysts in which ammonia solution was used as a precipitant. Because the ammonia solution is a weak base and violently evaporates in the synthesis process, the pH value of this solution was maintained at 9.

Upon completion of the precipitation reaction, the precipitated solids were filtered, washed and dried at 110 °C overnight. The dried solids were subsequently calcined at 650 °C for 6 h. The prepared Ni-Al_2O_3 catalysts were denoted as Ni50-X, where X represents the type of precipitant: urea, Na_2CO_3, NaOH, K_2CO_3, KOH or NH_4OH. The nickel content of all of the catalysts was fixed at 50 wt.%.

2.2. Characterization

Nitrogen adsorption–desorption isotherms for the catalysts were obtained on a BELsorp (BEL Japan) instrument, and the specific surface area of the catalysts was determined using the Brunauer–Emmett–Teller (BET) method. The crystalline structures of the catalysts were investigated using XRD (D-Max 2500, Rigaku). To identify metal-support interactions in the catalysts, temperature-programmed reduction (TPR) measurements (BELCAT-B, BEL Japan) were conducted at temperatures that ranged from room temperature to 1000 °C at a heating rate of 5 °C min^{-1}. For the TPR measurements, 10% H_2 in Ar gas (50 mL-STP min^{-1}) was used to evaluate 0.1 g of the catalyst.

Hydrogen chemisorption data (BEL-METAL-3, BEL Japan) were measured to investigate the nickel dispersion and nickel surface area of the catalysts. Prior to the chemisorption measurements, 30 mg of the catalysts was reduced with pure H_2 gas (50 mL-STP min^{-1}) at 700 °C for 1 h. The hydrogen uptake was determined by periodically injecting a mixed gas (20% H_2 in Ar) into the reduced catalyst. The nickel dispersion and nickel surface area were calculated by assuming that one hydrogen atom occupies one surface nickel atom and that the cross-sectional area of the atomic nickel was 6.49×10^{-20} m^2 Ni-$atom^{-1}$. A scanning electron microscope (FE-SEM, S4700 and S4800, Hitachi) was also used to investigate the morphology of particles in the prepared catalysts.

2.3. Electrolyte poisoning of catalysts

In DIR-MCFC stacks, electrolytes (mixtures of Li_2CO_3 and K_2CO_3) tend to severely deactivate internal reforming catalysts. To investigate the effect of electrolyte poisoning on the catalytic activity, the catalysts were artificially poisoned with an electrolyte solution using the excess-water impregnation method. First, the catalysts were crushed into 60–100 mesh granules (150–250 μm), which were then mixed with the electrolyte solution in a flask. Water was extracted from the flask using a rotary vacuum evaporator, and, after the vacuum drying was complete, the catalysts were dried at 110 °C for 2 h. The amount of electrolyte was fixed at 10 wt.% for all of the catalysts.

2.4. Steam reforming of methane

The steam reforming of methane over the Ni-Al_2O_3 catalysts was performed at reaction temperatures of 650 °C under atmospheric pressure, which are the same operating conditions employed for the DIR-MCFC. The catalyst (5 mg, 60–100 mesh granules) and dilute α-Al_2O_3 (100 mg, 60–100 mesh granules) were placed in a fixed-bed quartz reactor (I.D. = 4 mm) after being well mixed in the vessel. The thermocouple was placed in the top one-third of the catalyst bed. Before the methane reforming reaction was initiated, the catalyst was reduced at 700 °C for 1 h under a mixture of 10% H_2 in N_2 (100 mL-STP min^{-1}). The CH_4 and H_2O (vapor) reactants were supplied at 4 GHSV (gas hourly space velocity) regions. The CH_4 and H_2O flow rates and other conditions in the GHSV regions are listed in Table 1. The H_2O/CH_4 molar ratio was fixed at 2. The steam was prepared using an electric heater controlled at 200 °C before it was mixed with the other reactants.

The reforming reaction was stabilized at 650 °C for 1 h, and the GHSV was subsequently changed from region 1 to region 4. The catalytic activity measurements of each GHSV region were performed for 1 h. The reaction products were periodically sampled and

Table 1
Conditions in the GHSV regions at flow rates of CH_4 and H_2O (vapor).

Region	GHSV (h^{-1})	CH_4 (mL-STP min^{-1})[a]	H_2O (mL-STP min^{-1})[a]
Region 1	1,360,800	37.5	75
Region 2	2,721,600	75	150
Region 3	4,082,400	112.5	225
Region 4	5,443,200	150	300

[a] Standard conditions (0 °C, 1 atm).

analyzed using an in-line gas chromatograph (Agilent 3000) equipped with a TCD.

3. Results and discussion

3.1. Characterization of the prepared catalysts

The physical properties of the Ni-Al_2O_3 catalysts were examined via nitrogen isotherm measurements. Fig. 1 shows the nitrogen adsorption–desorption isotherms of the catalysts prepared using the co-precipitation method with different precipitants. All of the catalysts exhibited type-IV isotherms, which suggests that all of the catalysts prepared by the co-precipitation method are composed of well-developed mesopores [20,24]. However, the prepared catalysts exhibited different starting points and hysteresis-loop shapes.

Fig. 2 shows the pore size distribution of the catalysts with various precipitants in terms of the pore surface area and the pore volume. For the pore size distribution of pore surface area and pore volume (Fig. 2), the peak of the pore size was different for each prepared catalyst. In Fig. 2(a), the peaks of the pore sizes with respect to the pore surface area for the Ni50-urea, Ni50-Na_2CO_3, Ni50-NaOH, Ni50-K_2CO_3, Ni50-KOH and Ni50-NH_4OH catalysts appeared at approximately 4, 5, 7, 5, 7 and 10 nm, respectively. In Fig. 2(b), the peaks of the pore sizes with respect to the pore volume for the Ni50-urea, Ni50-Na_2CO_3, Ni50-NaOH, Ni50-K_2CO_3, Ni50-KOH and Ni50-NH_4OH catalysts appeared at approximately 50, 30, 8, 50, 7 and 12 nm, respectively.

The physisorption measurement results for each catalyst prepared using different precipitants are summarized in Table 2. The Ni50-urea catalyst exhibited the largest specific surface area, 210 m^2 $g\text{-}cat^{-1}$, and highest pore volume, 0.77 cm^3 $g\text{-}cat^{-1}$. The Ni50-NH_4OH catalyst exhibited the lowest specific surface area, 127 m^2 $g\text{-}cat^{-1}$, and the Ni50-KOH catalyst exhibited the lowest pore volume, 0.31 cm^3 $g\text{-}cat^{-1}$.

The catalysts prepared using precipitants that contained carbonate ions (i.e., the Ni50-urea, Ni50-Na_2CO_3 and Ni50-K_2CO_3 catalysts) exhibited higher pore volumes than the catalysts prepared with precipitants that contained hydroxide ions, (i.e., Ni50-NaOH, Ni50-KOH, Ni50-NH_4OH catalysts). The formation of a hysteresis loop affects the pore size and the pore volume [27,28]. In Fig. 1, the hysteresis loop of the catalysts prepared with precipitants that contained carbonate ions appeared at relative pressures greater than 0.7. The hysteresis loop of catalysts prepared using precipitants that contained hydroxide ions appeared at relative pressures between 0.5 and 0.95. In Fig. 2(a), the catalysts prepared with precipitants that contained hydroxide ions exhibited high intensities of smaller pore size regions in the pore size distribution curve of the pore surface area. In pore size distribution curves of pore volumes (Fig. 2(b)), the catalysts prepared with precipitants that contained carbonate ions displayed high intensities of pore sizes of 30–50 nm. Furthermore, these catalysts exhibited higher adsorbed nitrogen volumes in the nitrogen adsorption–desorption isotherms. These results indicate that the catalysts prepared with precipitants that contained carbonate ions exhibit greater pore sizes and higher pore volumes than do the catalysts prepared with precipitants that contained hydroxide ions. Specially, the Ni50-urea catalyst exhibits the highest pore volume in Figs. 1, 2(b) and Table 2. These results indicate that the type of precipitant affects the physical properties of the formed catalysts.

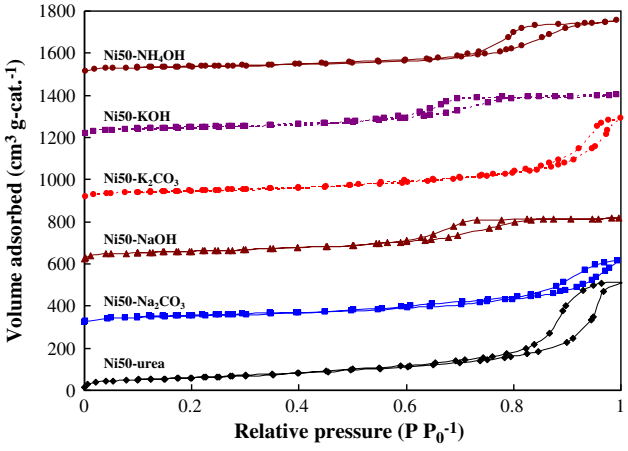

Fig. 1. Nitrogen adsorption–desorption isotherms for catalysts prepared using various precipitants. The adsorption–desorption data for Ni50-urea, Ni50-Na_2CO_3, Ni50-NaOH, Ni50-K_2CO_3, Ni50-KOH and Ni50-NH_4OH were vertically offset by 0, 300, 600, 900, 1200 and 1500 cm^3 $g\text{-}cat^{-1}$, respectively.

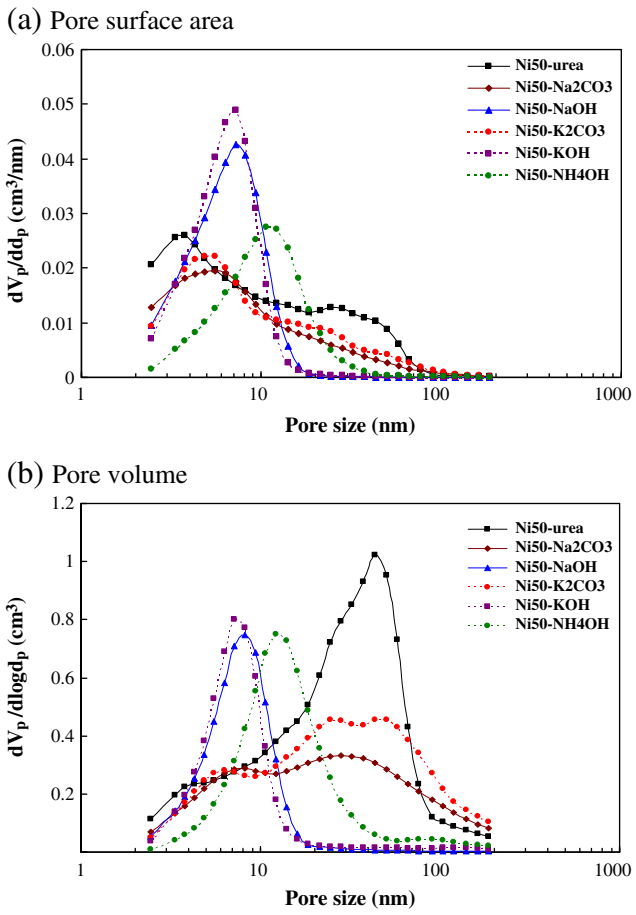

Fig. 2. The pore size distribution for catalysts prepared using various precipitants.

Table 2
Physisorption results of catalysts prepared via co-precipitation using various precipitants.

Sample	Specific surface area (m^2 $g\text{-}cat^{-1}$)	Pore volume (cm^3 $g\text{-}cat^{-1}$)	Average pore size (nm)
Ni50-urea	210	0.77	15
Ni50-Na_2CO_3	183	0.47	10
Ni50-NaOH	206	0.33	6
Ni50-K_2CO_3	163	0.57	14
Ni50-KOH	169	0.31	7
Ni50-NH_4OH	127	0.40	13

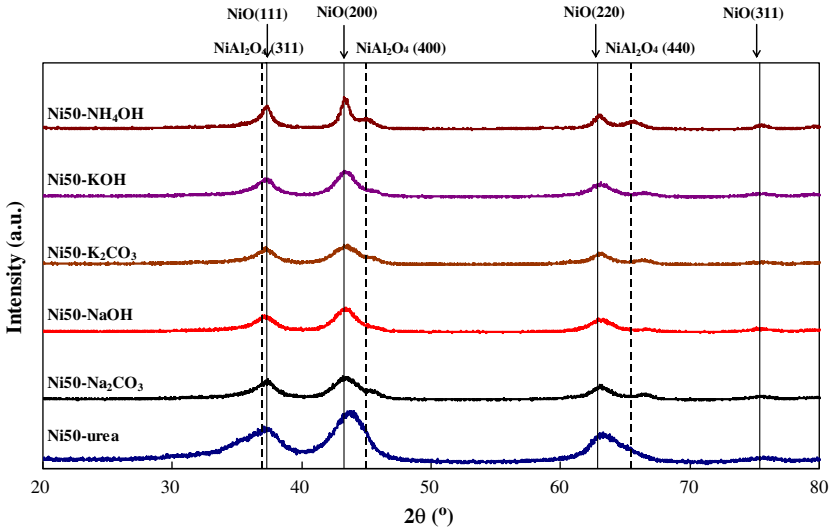

Fig. 3. XRD patterns for catalysts prepared via co-precipitation using various precipitants after calcination at 650 °C for 6 h.

Fig. 3 shows the XRD patterns of catalysts prepared via co-precipitation using various precipitants after calcination at 650 °C for 6 h. All of the catalysts, except the Ni50-urea catalyst, exhibited strong diffraction peaks that correspond to NiO and weak peaks that correspond to $NiAl_2O_4$. The Ni50-urea catalyst exhibited only strong diffraction peaks that correspond to NiO. The Ni50-NH_4OH catalyst exhibited stronger diffraction peaks that correspond to the $NiAl_2O_4$ crystal lattice than did the other prepared catalysts.

Fig. 4 shows the XRD patterns of the catalysts after they were reduced at 700 °C for 1 h. All of the catalysts exhibited strong peaks that correspond to metallic Ni crystals and weak diffraction peaks that correspond to $NiAl_2O_4$ and γ-Al_2O_3. In particular, the Ni50-urea catalyst exhibited strong peaks that correspond to metallic Ni crystals at Ni(111) and Ni(200), which suggests that the NiO was almost completely reduced to metallic Ni. This catalyst displayed lower peak intensity than did the other catalysts, which indicates a small crystallite size of metallic Ni. Other catalysts displayed indistinct diffraction peaks that correspond to $NiAl_2O_4$ and γ-Al_2O_3 at approximately $2\theta = 66°$. These results indicate that $NiAl_2O_4$ was not completely reduced to Ni and γ-Al_2O_3 [9].

The sizes of the crystalline metallic Ni domains were calculated from the XRD diffraction peaks of the reduced catalysts using the Scherrer equation, as shown in Table 3. The Ni50-urea catalyst exhibited the smallest size of crystalline metallic Ni, and the Ni50-KOH catalyst exhibited the largest size of crystalline metallic Ni. It is evident that the type of precipitant affects both the structure of the catalysts and the Ni crystallite size in the catalysts after reduction (Fig. 4 and Table 3).

TPR measurements were performed to investigate the interaction between the Ni species and the support and to test the reducibility of the catalysts. Fig. 5 shows the TPR profiles of the catalysts prepared in this study. All of the catalysts, with the exception of the Ni50-NH_4OH catalyst, exhibited reduction peaks between 650 and 720 °C, which indicate that the Ni species interact strongly with the Al_2O_3 support [26,29,30]. The Ni50-NH_4OH catalyst exhibited a small reduction peak at approximately 590 °C and a main reduction peak at approximately 750 °C. This result is caused by the formation of $NiAl_2O_4$ crystals in the catalyst (Fig. 3). The $NiAl_2O_4$ crystals in the Ni-Al_2O_3 catalyst are known to be a strong combination of NiO and Al_2O_3 species and exhibited a reduction peak at high temperature

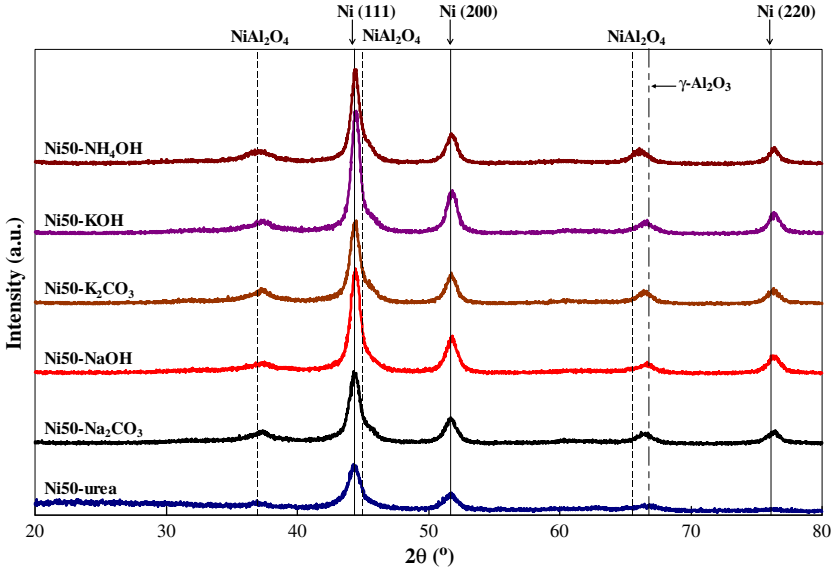

Fig. 4. XRD patterns for catalysts prepared via co-precipitation using various precipitants after reduction at 700 °C for 1 h.

Table 3
Crystalline size of metallic Ni in the Ni-Al_2O_3 catalysts reduced at 700 °C for 1 h.

Sample	Crystalline size of metallic Ni (nm)[a]
Ni50-urea	6.2
Ni50-Na_2CO_3	8.5
Ni50-NaOH	8.2
Ni50-K_2CO_3	8.8
Ni50-KOH	9.5
Ni50-NH_4OH	9.2

[a] Calculated from the broadening of the Ni(200) diffraction peak in Fig. 4.

(approximately 800 °C) [29,31]. Thus, the main reduction peak of the Ni50-NH_4OH catalyst is shifted at approximately 750 °C. In addition, a small reduction peak at 590 °C results from weaker interactions between the Ni species and the support than those of other catalysts.

Hydrogen chemisorption was performed to identify the Ni dispersion and the Ni surface area in the prepared catalysts. Table 4 summarizes the hydrogen chemisorption results. The Ni dispersion is defined as the ratio between the Ni particles exposed to reactants and the total Ni contained in the catalyst [26]. Because a higher Ni dispersion and a larger Ni surface area usually result in more active catalysts, it is desirable to maximize the Ni dispersion and Ni surface area of a given catalyst. The Ni50-urea catalyst exhibited the highest Ni dispersion and the largest Ni surface area, and the Ni50-NH_4OH catalyst exhibited the lowest values. Hydrogen chemisorption results are related to the specific surface area of the prepared catalysts (Table 2). In general, the catalysts with large specific surface areas tend to exhibit high values of Ni dispersion and large Ni surface areas [7,24].

Fig. 6 shows the SEM images of the prepared catalysts. The morphologies of the particles in the Ni50-urea, Ni50-Na_2CO_3 and Ni50-K_2CO_3 catalysts were petal-like shapes. In general, spherical particles were observed in the Ni50-NaOH, Ni50-KOH and Ni50-NH_4OH catalysts prepared with precipitants that contained hydroxide ions. The particle morphology depends on the components of the catalyst precursors and differed according to the functional group of the precipitants (carbonate or hydroxide ions). The carbonate ions in precipitants reacted with nickel and aluminum species and formed hydrotalcite-like (layered double hydroxide (LDH): $Ni_{(1-x)}Al_x(OH)_2(CO_3)$) structures during the precipitation reactions [25,26,32]. In contrast, the hydroxide ions in precipitants formed metal-hydroxide ($Ni_{(1-x)}Al_x(OH)_2$) structures during the precipitation reactions. The catalysts prepared with precipitants that contain carbonate ions (i.e., the Ni50-urea, Ni50-Na_2CO_3 and Ni50-K_2CO_3 catalysts) are expected to exhibit higher pore volume due to the petal-like particles than are

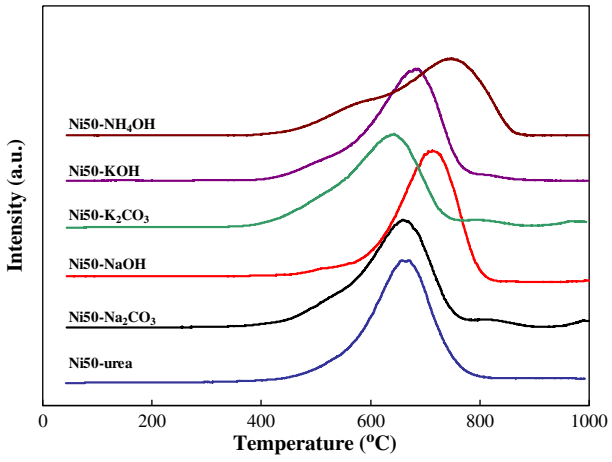

Fig. 5. TPR profiles for catalysts prepared via co-precipitation using various precipitants.

Table 4
Hydrogen chemisorption results of catalysts prepared via co-precipitation using various precipitants.

Sample	Amount of hydrogen uptake (mmol g-cat^{-1})	Ni dispersion (%)	Ni surface area (m^2 g-cat^{-1})
Ni50-urea	0.30	6.5	22
Ni50-Na_2CO_3	0.20	4.7	16
Ni50-NaOH	0.22	5.2	17
Ni50-K_2CO_3	0.19	4.4	15
Ni50-KOH	0.16	3.8	13
Ni50-NH_4OH	0.09	2.2	7

the catalysts prepared with precipitants that contain hydroxide ions (i.e., the Ni50-NaOH, Ni50-KOH and Ni50-NH_4OH catalysts). These results are confirmed by the data in Table 2.

3.2. Steam reforming of methane over the prepared catalysts

Fig. 7 shows the catalytic activities for methane steam reforming over the fresh Ni-Al_2O_3 catalysts prepared using various precipitants. The methane conversions and reaction rates for methane steam reforming were calculated for a reaction temperature of 650 °C, which is consistent with the operating temperature of DIR-MCFCs. The flow rate of reactants was varied within ranges consistent with the reaction conditions, which are classified into GHSVs with 4 total regions (Table 1). In Fig. 7 (a), the methane conversions of the prepared catalysts decreased with an increase in the GHSV. However, in Fig. 7(b), the reaction rates of the prepared catalysts increased with an increase in the GHSV.

In the low GHSV region (region 1), all of the prepared catalysts exhibited similar methane conversions and reaction rates, which were greater than 90% and 5.0 mmol CH_4 g-cat^{-1} s^{-1}, respectively. In GHSV regions 2 to 4, however, the prepared catalysts exhibited different catalytic activities as the GHSV was increased. In the case of the Ni50-NaOH, Ni50-KOH and Ni50-NH_4OH catalysts, the methane conversion rates decreased rapidly with increasing GHSV (Fig. 7(a)). The reaction rates barely increased between GHSV regions 2 and 4 (Fig. 7(b)). For the Ni50-NaOH and Ni50-KOH catalysts, changes in the reaction rates were not observed between GHSV regions 3 and 4. Thus, the maximum reaction rates of the Ni50-NaOH and Ni50-KOH catalysts are found at these regions (i.e., 8.11 and 8.05 mmol CH_4 g-cat^{-1} s^{-1}, respectively). In contrast, the catalysts prepared with precipitants that contained carbonate ions (i.e., the Ni50-urea, Ni50-Na_2CO_3 and Ni50-K_2CO_3 catalysts) exhibited a relatively slow decrease in methane conversion with an increase in the GHSV region (Fig. 7(a)), and reaction rates increased with an increase in the GHSV region (Fig. 7(b)). Thus, the maximum reaction rates of these catalysts were not found. The Ni50-K_2CO_3 catalyst, in particular, displayed the highest catalytic activity, and the Ni50-urea catalyst displayed the second-highest catalytic activity.

The mechanisms by which the components of the electrolytes in DIR-MCFCs (mixtures of Li_2CO_3 and K_2CO_3) contaminate the reforming catalysts have been reported elsewhere [7,8,10–16]. Thus, the present study is focused on improving the poisoning resistance toward deactivation by the electrolyte for the Ni-Al_2O_3 catalysts prepared via the co-precipitation method using various precipitants. Fig. 8 shows the catalytic activities for methane steam reforming over the Ni-Al_2O_3 catalysts poisoned with 10 wt.% electrolyte. The methane conversions and reaction rates for methane steam reforming were measured at 650 °C. In Fig. 8, the Ni50-urea catalyst exhibited the highest catalytic activities in all GHSV regions, and the Ni50-KOH catalyst exhibited the lowest catalytic activities in all GHSV regions. The methane conversions of the prepared catalysts decreased with an increase in the GHSV region in Fig. 8(a), and the reaction rates of the prepared catalysts slowly increased between GHSV regions 2 and 4 in Fig. 8(b). The reaction rates of the Ni50-NaOH

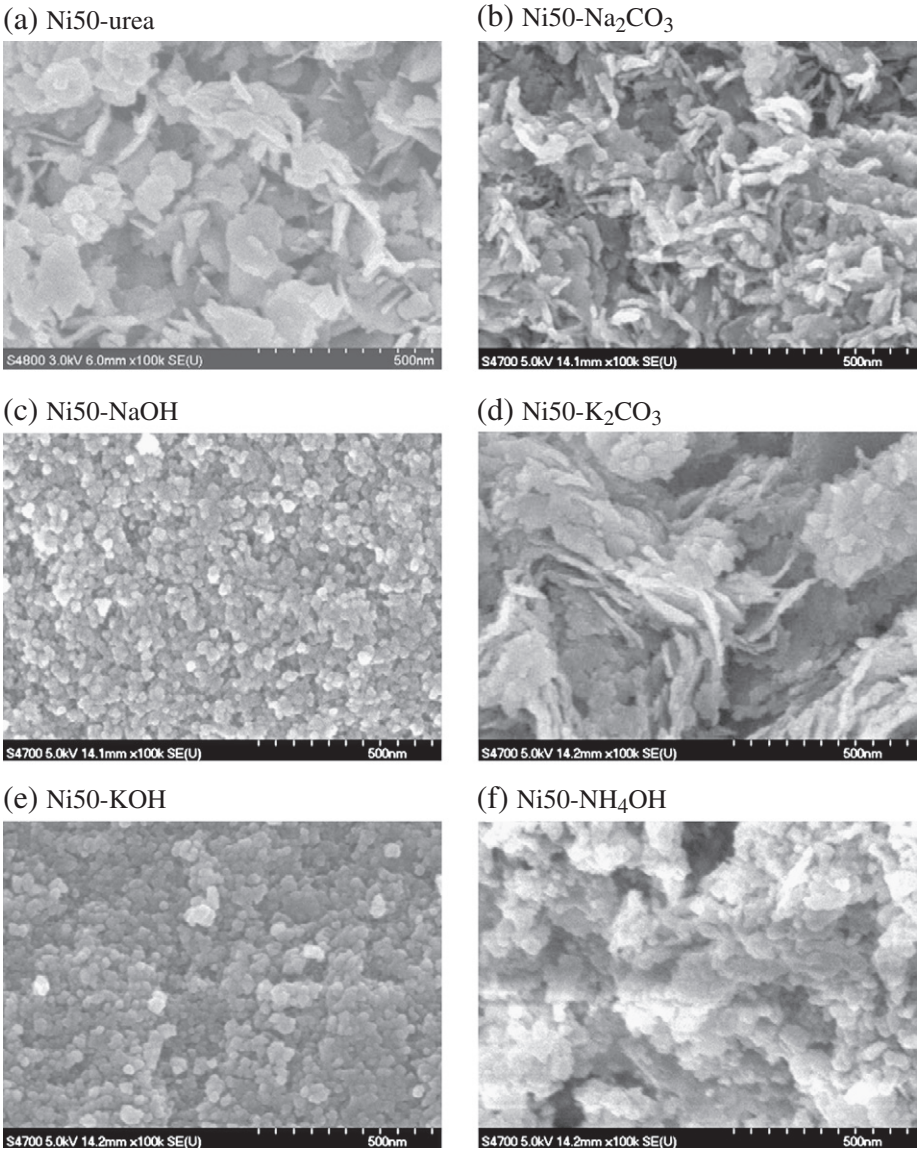

Fig. 6. SEM images of catalysts prepared via co-precipitation using various precipitants after calcination at 650 °C for 6 h.

and Ni50-KOH catalysts, in particular, barely increased in all GHSV regions. The catalysts prepared with precipitants that contained carbonate ions exhibited higher catalytic activities than did the catalysts prepared with precipitants that contained hydroxide ions in both the fresh and poisoned states (Figs. 7 and 8). The Ni50-urea and Ni50-K_2CO_3 catalysts exhibited particularly good catalytic activities for methane steam reforming in both the fresh and poisoned states.

Fig. 9 shows a comparison of the catalytic activities and physicochemical properties between the fresh and poisoned catalysts. The catalytic activities are calculated at GHSV region 3. The relevant physicochemical properties of the catalysts are the pore volumes and the nickel surface areas. The Ni50-urea, Ni50-Na_2CO_3 and Ni50-K_2CO_3 catalysts, which are the catalysts prepared using precipitants that contained carbonate ions, exhibited relatively high methane conversion and reaction rates for methane steam reforming in both the fresh and poisoned states. These catalysts exhibited pore volumes that were relatively higher than those of the catalysts prepared using precipitants that contained hydroxide ions (Table 2). In the fresh state, the Ni50-K_2CO_3 catalyst exhibited the highest catalytic activity despite exhibiting the second-highest pore volume ($0.57\ cm^3\ g\text{-}cat^{-1}$), and this catalyst also exhibited a relatively low nickel surface area of $15\ m^2\ g\text{-}cat^{-1}$. In contrast, the Ni50-urea catalyst exhibited the second-highest catalytic activity despite exhibiting the highest pore volume and nickel surface area ($0.77\ cm^3\ g\text{-}cat^{-1}$ and $22\ m^2\ g\text{-}cat^{-1}$, respectively). In the poisoned state, however, the Ni50-urea catalyst exhibited the highest catalytic activity, and the Ni50-K_2CO_3 catalyst exhibited the second-highest catalytic activity. The catalytic activity of the Ni50-K_2CO_3 catalyst between the fresh and poisoned states was decreased to a greater extent than that of the Ni50-urea catalyst. The performances of the prepared catalysts in the fresh and poisoned states are ranked according to the pore volumes of the catalysts without reference to the nickel surface areas. These results indicate that the activities of the prepared catalysts in the fresh and poisoned states are related to the pore volumes of the catalysts.

When the flow rates of reactants are high, a large quantity of reactants can be diffused into the catalyst and contact the active sites, which results in a high catalytic activity. For this phenomenon to occur, the catalyst must exhibit a high pore volume and a large nickel surface area. A high pore volume depends on the existence of well-developed mesopores, which enable the reactants to easily contact the active sites. For example, the Ni50-NH_4OH catalyst displayed a

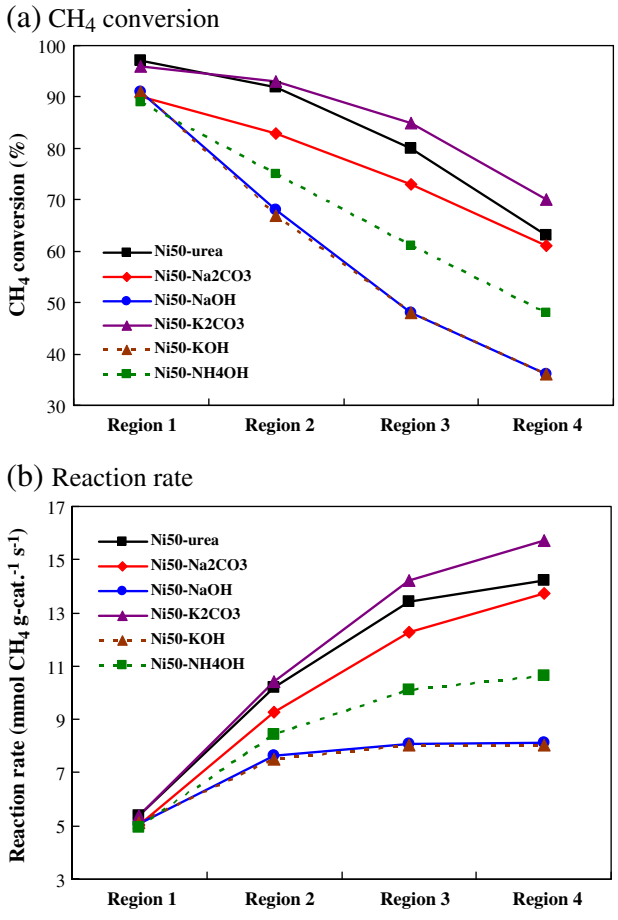

Fig. 7. (a) CH_4 conversion and (b) reaction rate for methane steam reforming over fresh Ni-Al_2O_3 catalysts prepared via co-precipitation using various precipitants.

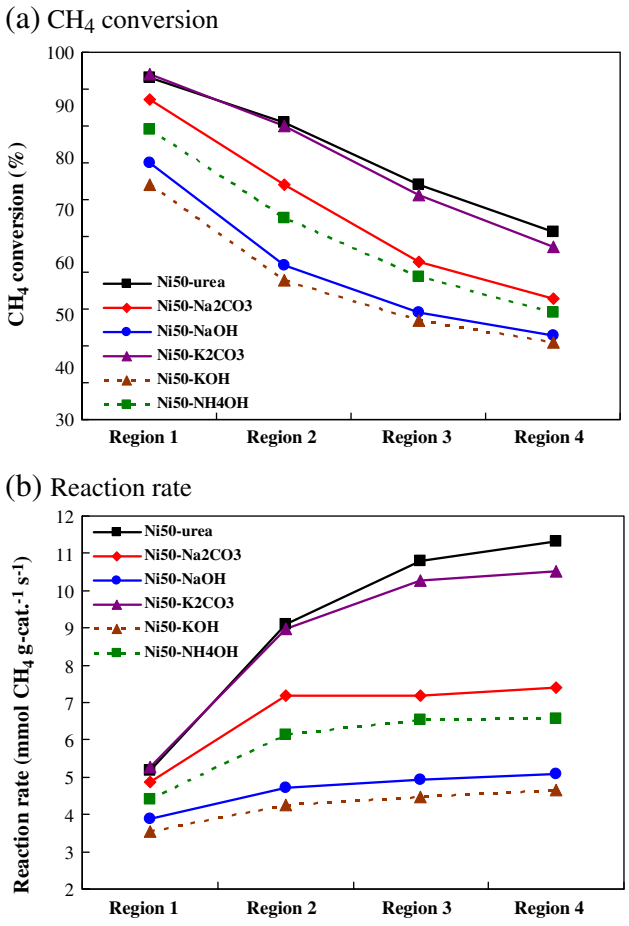

Fig. 8. (a) CH_4 conversion and (b) reaction rate for methane steam reforming over Ni-Al_2O_3 catalysts poisoned with 10 wt.% electrolyte.

middle ranking of catalytic activity despite exhibiting the lowest nickel surface area among the investigated catalysts. The Ni50-NaOH catalyst had the second-highest nickel surface area; however, the catalytic activity and pore volume were the second-lowest such values. Furthermore, a ranking of the catalytic activities showed that the pore volumes of the prepared catalysts, without regard to the nickel surface areas, were approximately the same. These results indicate that a high pore volume and a large nickel surface area in the catalyst are necessary conditions; however, the pore volume is more influential for high catalytic activity at high GHSV regions than is the nickel surface area. The characteristics of a high pore volume are an increase in the diffusion rate of the reactants and an assisted contact between the reactants and the active sites in the catalyst.

The catalysts prepared using precipitants that contained carbonate ions exhibited high pore volumes and pore sizes with high catalytic activities. These catalysts were formed by calcination of hydrotalcite-like (layered double hydroxide (LDH): $Ni_{(1-x)}Al_x(OH)_2CO_3$) structures which are precipitates formed through reaction between metal nitrate solutions and precipitants that contained carbonate ions. On the other hand, the catalysts prepared using precipitants that contained hydroxide ions exhibited low pore volumes and pore sizes with low catalytic activities. These catalysts were formed by calcination of metal-hydroxide ($Ni_{(1-x)}Al_x(OH)_2$) which is precipitate formed through reaction between metal nitrate solutions and precipitants that contained hydroxide ions. After calcination process, the hydrotalcite-like structures changed to Ni-Al_2O_3 catalyst of petal-like shape with many vacancies and metal-hydroxide changed to Ni-Al_2O_3 catalyst of dense sphere shape in SEM images (Fig. 6). Thus, Ni-Al_2O_3 catalyst of petal-like shape may have high pore volumes and pore sizes (Table 2). And these effects may influence the performance of catalysts.

In the SEM image (Fig. 6), also, the catalysts prepared using precipitants that contained carbonate ions showed petal-like shapes with many vacancies, and these catalysts exhibited high catalytic activities due to high pore volumes. These results indicate that the precipitants that contained carbonate ions affect the morphology of catalysts during the synthesis process, and these effects may strongly assist the development of mesopores and enhance the pore volume; in particular, precipitants that contain urea and potassium carbonate (K_2CO_3) are extremely effective.

A strong resistance to deactivation by the electrolyte is crucial for the reforming catalyst in a DIR-MCFC. The present study suggests that the catalysts prepared with precipitants that contain carbonate ions exhibit higher pore volumes and higher catalytic activities than the catalysts prepared with precipitants that contain hydroxide ions. In particular, the Ni50-urea catalyst exhibits the best physicochemical properties and the highest catalytic activity while simultaneously exhibiting a strong resistance toward contamination by the electrolyte.

4. Conclusions

Ni-Al_2O_3 catalysts are prepared via the co-precipitation method using various precipitants: urea, Na_2CO_3, NaOH, K_2CO_3, KOH and NH_4OH. The effects of the precipitants on the physicochemical properties and catalytic activities of the Ni-Al_2O_3 catalysts are investigated. The Ni50-urea catalyst, in which urea was used as a precipitant, exhibits the highest specific surface area and the greatest pore volume. In the XRD patterns of catalysts calcined at 650 °C for

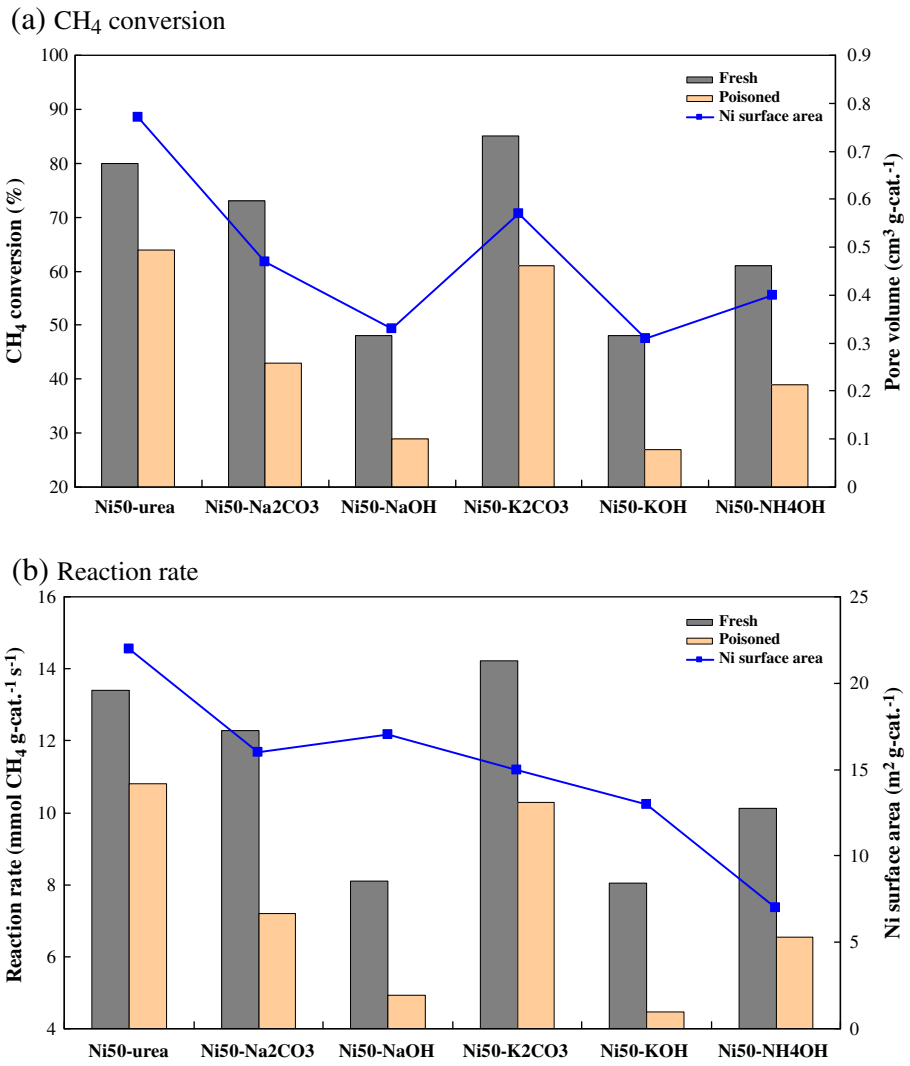

Fig. 9. Comparison of catalytic activities and physicochemical properties between fresh and poisoned catalysts. The catalytic activities are calculated at region 3.

6 h, all of the catalysts, with the exception of the Ni50-urea catalyst, exhibit strong diffraction peaks that correspond to NiO and weak peaks that correspond to $NiAl_2O_4$. The TPR profiles of the catalysts, with the exception of profile of the Ni50-NH_4OH catalyst, showed reduction peaks between 650 and 720 °C. These results indicate that the Ni species interact strongly with the Al_2O_3 support. The chemisorption results indicate that the Ni50-urea catalyst exhibits the highest Ni dispersion and the highest Ni surface area. The Ni50-urea and Ni50-K_2CO_3 catalysts exhibit high pore volumes and good catalytic activities for methane steam reforming. The Ni50-urea catalyst, in particular, exhibits the best physicochemical properties and a good catalytic activity combined with a strong resistance toward contamination by the electrolyte.

Acknowledgments

This work was supported by the New & Renewable Energy program of the Korea Institute of Energy Technology Evaluation and Planning (KETEP) grant, which was funded by the Ministry of Knowledge Economy of Korea (2008-N-FC12-J-04-2100).

References

[1] M. Bischoff, Journal of Power Sources 160 (2006) 842–845.
[2] R. Rashidi, P. Berg, I. Dincer, International Journal of Hydrogen Energy 34 (2009) 4395–4405.
[3] J.R. Rostrup-Nielsen, L.J. Christiansen, Applied Catalysis A: General 126 (1995) 381–390.
[4] X. Deng, J. Sun, S. Yu, J. Xi, W. Zhu, X. Qiu, International Journal of Hydrogen Energy 33 (2008) 1008–1013.
[5] D. Li, Y. Nakagawa, K. Tomishige, Applied Catalysis A: General 408 (2011) 1–24.
[6] H.S. Roh, Y.S. Jung, K.Y. Koo, U.H. Jung, Y.S. Seo, W.L. Yoon, Chemical Society of Japan 38 (2009) 1162–1163.
[7] K. Park, K.Y. Kim, L. Lu, T.H. Lim, S.A. Hong, H.I. Lee, Fuel Cells 7 (2007) 211–217.
[8] H.S. Roh, Y.S. Jung, K.Y. Koo, U.H. Jung, Y.S. Seo, W.L. Yoon, Applied Catalysis A: General 383 (2010) 156–160.
[9] Y.S. Jung, W.L. Yoon, T.W. Lee, Y.W. Rhee, Y.S. Seo, International Journal of Hydrogen Energy 35 (2010) 11237–11244.
[10] A.L. Dick, Journal of Power Sources 71 (1998) 111–122.
[11] D.S. Park, Z. Li, H. Devianto, H.I. Lee, International Journal of Hydrogen Energy 35 (2010) 5673–5680.
[12] M. Matsumura, C. Hirai, Journal of Chemical Engineering of Japan 31 (1998) 734–740.
[13] R.J. Berger, E.B.M. Doesburg, J.G. van Ommen, J.R.H. Ross, Applied Catalysis A: General 143 (1996) 343–365.
[14] K. Sugiura, T. Yodo, M. Yamauchi, K. Tanimoto, Journal of Power Sources 157 (2006) 739–744.
[15] M. Ito, T. Tagawa, S. Goto, Applied Catalysis A: General 184 (1999) 73–80.
[16] S.H. Clarke, A.L. Dicks, K. Pointon, T.A. Smith, A. Swann, Catalysis Today 38 (1997) 411–423.
[17] N. Salhi, A. Boulahouache, C. Petit, A. Kiennemann, C. Rabia, International Journal of Hydrogen Energy 36 (2011) 11433–11439.
[18] A.E.C. Luna, M.E. Iriarte, Applied Catalysis A: General 343 (2008) 10–15.
[19] J.G. Seo, M.H. Youn, J.C. Jung, I.K. Song, International Journal of Hydrogen Energy 34 (2009) 5409–5416.
[20] J.G. Seo, M.H. Youn, S. Park, D.R. Park, J.C. Jung, J.S. Chung, I.K. Song, Catalysis Today 146 (2009) 44–49.

[21] K. Takehira, T. Shishido, P. Wang, T. Kosaka, K. Takaki, Journal of Catalysis 221 (2004) 43–54.
[22] H. Devianto, Z.L. Li, S.P. Yoon, J. Han, S.W. Nam, T.H. Lim, H.I. Lee, International Journal of Hydrogen Energy 35 (2010) 2591–2596.
[23] L. Garcia, A. Benedicto, E. Romeo, M.L. Salvador, J. Arauzo, R. Bilbao, Energy & Fuels 16 (2002) 1222–1230.
[24] J.G. Seo, M.H. Youn, D.R. Park, I. Nam, I.K. Song, International Journal of Hydrogen Energy 34 (2009) 8053–8060.
[25] H. Cheng, B. Yue, X. Wang, X. Lu, W. Ding, Journal of Natural Gas Chemistry 18 (2009) 225–231.
[26] Y.S. Seo, Y.S. Jung, W.L. Yoon, I.G. Jang, T.W. Lee, International Journal of Hydrogen Energy 36 (2011) 94–102.
[27] K.S.W. Sing, D.H. Everett, R.A.W. Haul, L. Moscou, R.A. Pierotti, J. Rouquerol, T. Siemieniewska, Pure and Applied Chemistry 57 (1998) 603–619.
[28] S.J. Gregg, K.S.W. Sing, Adsorption, Surface Area and Porosity, second ed., Academic Press Inc., London, 1982, pp. 111–194.
[29] G. Li, L. Hu, J.M. Hill, Applied Catalysis A: General 301 (2006) 16–24.
[30] O.W. Perez-Lopez, A. Senger, N.R. Marcilio, M.A. Lansarin, Applied Catalysis A: General 303 (2006) 234–244.
[31] J. Chen, Q. Ma, T.E. Rufford, Y. Li, Z. Zhu, Applied Catalysis A: General 362 (2009) 1–7.
[32] A. Romero, M. Jobbagy, M. Laborde, G. Baronetti, N. Amadeo, Catalysis Today 149 (2010) 407–412.